Materials Characterization 110 (2015) 236–241

Contents lists available at ScienceDirect

Materials Characterization

journal homepage: www.elsevier.com/locate/matchar

Microstructure and micro-texture evolution during large strain deformation of Inconel alloy IN718

Niraj Nayan [a], N.P. Gurao [b], S.V.S. Narayana Murty [a,*], Abhay K. Jha [a], Bhanu Pant [a], Koshy M. George [a]

[a] Materials and Mechanical Entity, Vikram Sarabhai Space Centre, Trivandrum 695 022, India
[b] Department of Materials Science and Engineering, Indian Institute of Technology, Kanpur 208 016, India

ARTICLE INFO

Article history:
Received 2 January 2015
Received in revised form 22 October 2015
Accepted 23 October 2015
Available online 27 October 2015

ABSTRACT

The hot deformation behaviour of Inconel alloy IN718 was studied in the temperature range of 950–1100 °C and at strain rates of 0.01 and 1 s^{-1} with a view to understand the microstructural evolution as a function of strain rate and temperature. For this purpose, a single hit, hot isothermal plane strain compression (PSC) technique was used. The flow curves obtained during PSC exhibited weak flow softening at higher temperatures. Electron backscattered diffraction analysis (EBSD) of the PSC tested samples at the location of maximum strain revealed dynamic recrystallisation occurring at higher temperatures. Based on detailed microstructure and microtexture analyses, it was concluded that single step, large strain deformation has a distinct advantage in the thermo-mechanical processing of Inconel alloy IN718.

1. Introduction

Nickel based superalloys have unique combination of properties such as strength retention at elevated temperatures coupled with resitance to high temperature oxidation, which makes them suitable for high temperature applications. Inconel alloy IN 718 is a precipitation-strengthened nickel based superalloy, having excellent creep resistance and high temperature oxidation resistance. In view of its excellent mechanical properties up to intermediate temperatures (650 °C) and processing versatility, this alloy is being widely used in the gas turbine industry for static structures as well as rotating disc and shaft components [1–6].

Optimisation of hot workability and control of microstructure are essential for obtaining products with repeatable properties in a manufacturing environment. The microstructural evolution in Inconel alloy IN718 is very sensitive to the thermo-mechanical processing parameters such as strain, strain rate and temperature. In order to establish the thermo-mechanical processing parameters to obtain the most desirable mechanical properties and microstructures, computer simulation of thermo-mechanical processing of IN7I8 has been carried out [7,8]. Therefore, it is important to study the effect of strain rate on the flow stress and microstructural evolution in Inconel alloy IN718 deformed to large strains.

Although there were many studies focused on the flow behaviour of Ni-based superalloys during bulk forming processes by means of uniaxial compression [9,10],] few investigations addressed the flow characteristics in forming process such as hot rolling. Uniaxial compression is widely used to simulate forging operations upto strains of unity, beyond which specimen barreling occurs leading to inhomogeneous deformation. On the other hand, large strains can be introduced into a specimen through plane strain compression testing and therefore PSC is particularly suited for the physical simulation of hot rolling, which is of major technological importance. Plane strain compression testing, first proposed by Orowan is a modified compression test which could simulate material flow behaviour experienced during rolling. The test was later popularized by Watts and Ford [11] and this was followed by rigorous assessment and validation of the test, both experimentally and numerically by Sellars et al. [12]. One of the useful outputs of the PSC test is the generation of numerical data for optimizing constitutive equations for predicting the flow behaviour and microstructural evolution. These are subsequently used in numerical models of industrial scale processes and those based on finite element methods.

In a plane strain compression test, strain gets localized at the center of the specimen and it varies from zero at the surface of the specimen to a maximum at the centre of the specimen. This enables observation of microstructures of specimens deformed to different strains under given test conditions. For this purpose, a single hit, hot isothermal plane strain compression testing has been used in the present study.

Therefore the purpose of the present study is twofold; firstly to study the large strain deformation behaviour by conducting hot isothermal, single hit, plane strain compression tests on Inconel alloy IN718 and study the stress–strain behaviour under large strain conditions; and secondly to evaluate the microstructure and micro-texture of the deformed specimens to understand the mechanism of deformation under plane strain conditions.

* Corresponding author.
E-mail address: susarla.murty@gmail.com (S.V.S. Narayana Murty).

http://dx.doi.org/10.1016/j.matchar.2015.10.027
1044-5803/

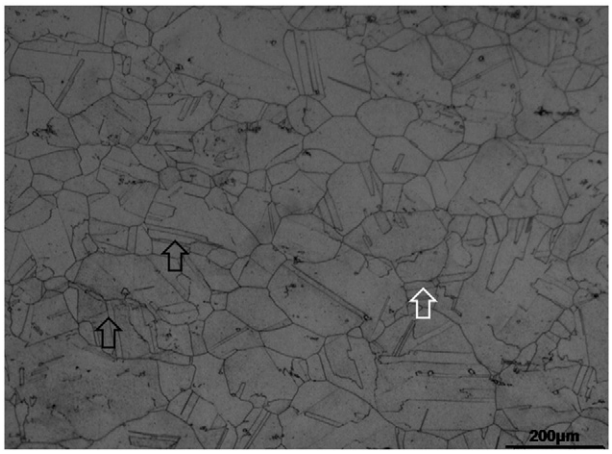

Fig. 1. Initial microstructure of the material used in the present study. The material is in as forged condition and has elongated grains in the direction of perpendicular to the direction of forging. The arrow marks indicate twin boundaries.

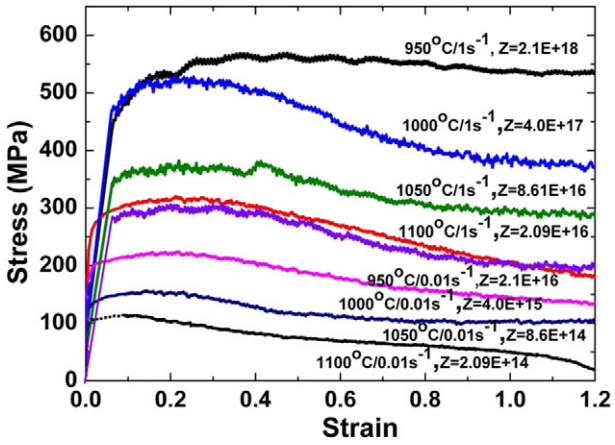

Fig. 3. Stress–strain curves of the plane strain compressed specimens deformed at different temperatures and strain rates.

2. Experimental

A large strain, single pass, simple compression technique extensively used by one of the co-authors [13–15] is utilized in the present study. In contrast to the other large strain deformation processes, where large strains are imposed by multi-pass deformation processes, this technique is a single pass deformation process. Therefore, this technique eliminates the possibility of the sample undergoing complex microstructural changes during static holding/reheating between the processing steps or avoids the sample undergoing complex multi-axial deformation. In the plane strain compression test used in the present study, the strain imposed gets concentrated at the center of the specimen and the strain varies in the range of 0–4 from the surface to the center of the specimen. This strain distribution facilitates the observation of microstructures of specimens deformed to various strain levels in a single specimen.

Test samples with dimensions of 15 mm (length) × 13 mm (width) × 12 mm (thickness) were fabricated from the hot rolled plate of IN718 superalloy. The specimens were machined in such a way that the compression axis is perpendicular to the rolling direction. The initial microstructure of the material used in the present study is shown in Fig. 1. The microstructure consisted of large equiaxed grains with a large number of twins where both grain and twin boundaries are straight with no sub-structural features. The X-ray diffractogram of the sample (Fig. 2) shows peaks for face centred cubic phase though the superalloy consists of γ and γ′ phases due to coherent nature of the γ′ precipitate. The superlattice peaks of the precipitates were not observed due to faster scanning speed.

Using a thermo-mechanical simulator (Gleeble 3500) capable of controlling the specimen temperature, strain and strain rate, plane strain compression tests were performed. In order to conduct the test, the specimens were heated to the desired temperature in the range of 950 °C to 1100 °C. Heating of the specimen was done at 5 K s^{-1} from ambient temperature to the specified temperature by direct resistance (Joule heating) and then compressed in a single stroke after soaking at the desired temperature for 60 s. The compressive deformation was carried out in the time periods of 1.38 s and 138 s so as to impose nominal strain rates of 1 s^{-1} and 0.01 s^{-1}, respectively. Immediately after the deformation, the specimens were in-situ water quenched. Post compression, specimens were cut from the sample by a slow speed diamond saw for optical microscopy and for EBSD analysis.

Specimens for EBSD analysis after plane strain compression testing were carefully polished through mechanical polishing followed by electro polishing with Struers A2 solution containing perchloric acid, ethanol, butoxy ethanol and distilled water. The electron back scattered diffraction system attached to a FEI Quanta scanning electron microscope was used in the present study. TSL OIM 6 data collection and analysis software were used to collect and process the orientation information.

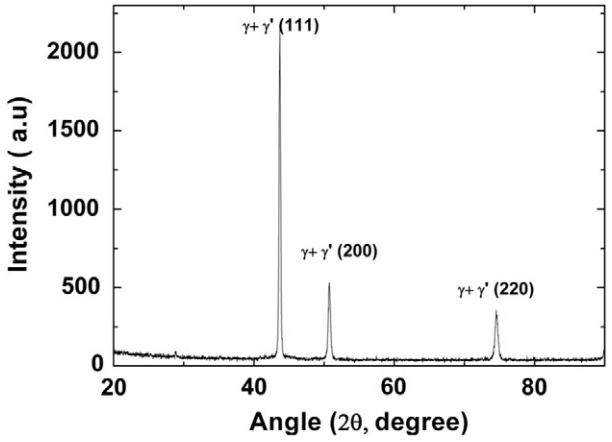

Fig. 2. X-ray diffractogram of the IN718 material under study.

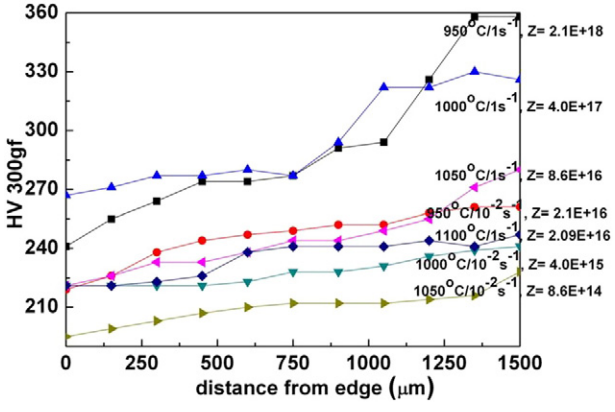

Fig. 4. Variation of vickers hardness with distance measures from the edge of the plane strain compression tested samples tested at various temperatures and strain rates.

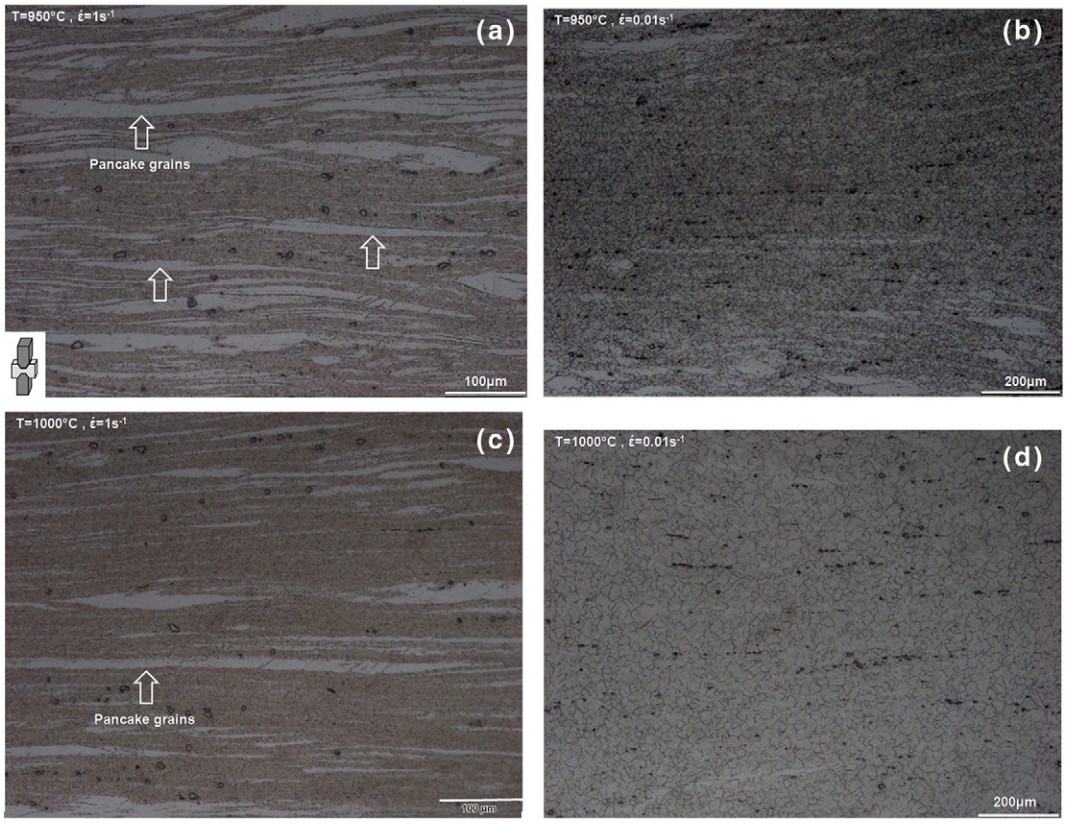

Fig. 5. Optical microstructures of specimens deformed at (a): 950 °C and 1 s^{-1}; (b): 950 °C and 0.01 s^{-1}; (c): 1000 °C and 1 s^{-1}; (d): 1000 °C and 0.01 s^{-1}. The microstructures are characterized by compressed grains without the evidence of any recrystallisation.

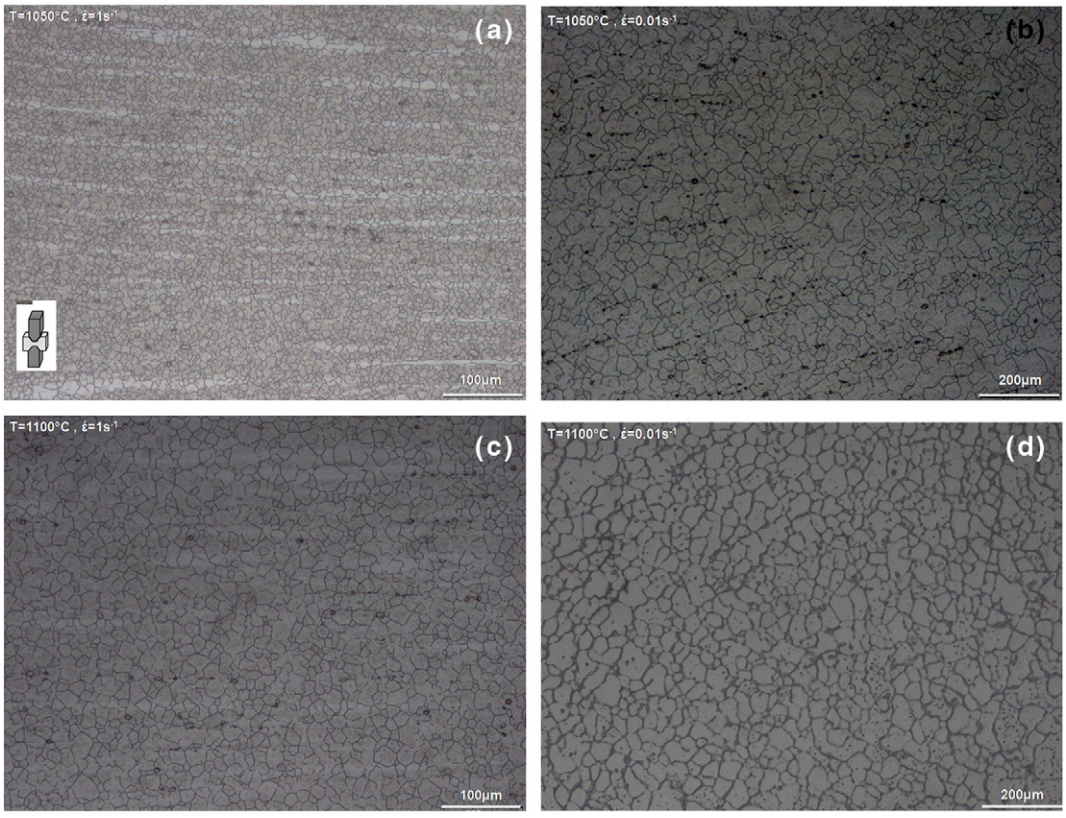

Fig. 6. Optical microstructures of specimens deformed at (a): 1050 °C and 1 s^{-1}; (b): 1050 °C and 0.01 s^{-1}; (c): 1100 °C and 1 s^{-1}; (d): 1100 °C and 0.01 s^{-1}. The microstructures are characterized by the evidence of clear recrystallised grains.

3. Results and discussion

3.1. Characteristics of flow curves

The microstructural evolution during hot deformation can be studied through the analysis of stress–strain curves [16–18]. The stress–strain curves obtained at various temperatures and strain rates of 0.01 and 1 s^{-1} are presented in Fig. 3. Further, to visualize the combined effect of strain rate and temperature on the flow behaviour of material, Zener-Holloman (Z) parameter defined as $Z = \dot{\varepsilon}\exp(Q/RT)$ was used and the Z values are also presented in Fig. 3. It can be clearly seen from Fig. 3 that the flow stress is very sensitive to test temperature and strain rates. The flow stress decreases monotonically with increase in temperature and decrease in strain rate.

In the early stage of deformation, strain hardening dominates which leads to increase in flow stress due to the combined effect of loading and temperature, work hardening and thermally activated softening mechanisms takes place simultaneously. The stress–strain curve can be divided into four parts based on the micro-mechanism taking place during loading. These stages are Stage I (Work hardening stage), Stage II (Transition stage), Stage III (Softening stage) and Stage IV (Steady stage). In stage I, the strain hardening due to pile of dislocations dominates over softening rate induced by dynamic recovery (DRV) and thus the stress rises steeply. Stage I is followed by stage II, where work hardening and softening phenomenon induced by dynamic recovery and recrystallization compete. In stage III, the stress drops steeply, which is due to dominance of dynamic recovery and dynamic recrystallization over strain hardening. Finally, in stage IV, the stress stabilizes due to balance between softening and hardening.

The presence of peak due to strain hardening is not distinct at lower Z values (below $Z = 4 \times 10^{15}$). The deformation at $Z = 2.1 \times 10^{18}$ is characterized by a complete balance between strain hardening and dynamic softening.

Based on the shape of stress–strain curves, it can be concluded that the mechanism of deformation at $Z = 2.1 \times 10^{18}$ is dynamic recovery whereas at lower Z values, it is dynamic recrystallisation.

Fig. 4 shows the variation of Vickers microhardness with distance from the edge of the plane strain compression tested samples tested under various Z conditions. The distance from the edge to the centre of the specimen is indicative of different strains from the edge ($\varepsilon = 0$) to the centre line ($\varepsilon = 4.0$). It can be seen from the figure that at all test temperatures and strain rates, work hardening type behaviour is observed with a common general trend being higher hardening with increasing Z parameter. It can be noticed from that for a given temperature, the sample deformed at higher strain rate has higher hardness. The hardness increase from the edge of the deformed sample to the centre line of the deformed sample is significantly higher for sample tested at higher stain rates as compared to that tested at lower stain rate.

3.2. Effect of strain on microstructural evolution

Fig. 5(a) and (c) show the optical microstructures of specimens deformed at 1 s^{-1} at 950 °C and 1000 °C respectively. The microstructures are characterized by compressed grains without the evidence of any recrystallisation. Presence of shear bands with intense deformation and elongated grains can also be noticed. Coarse slip bands in the

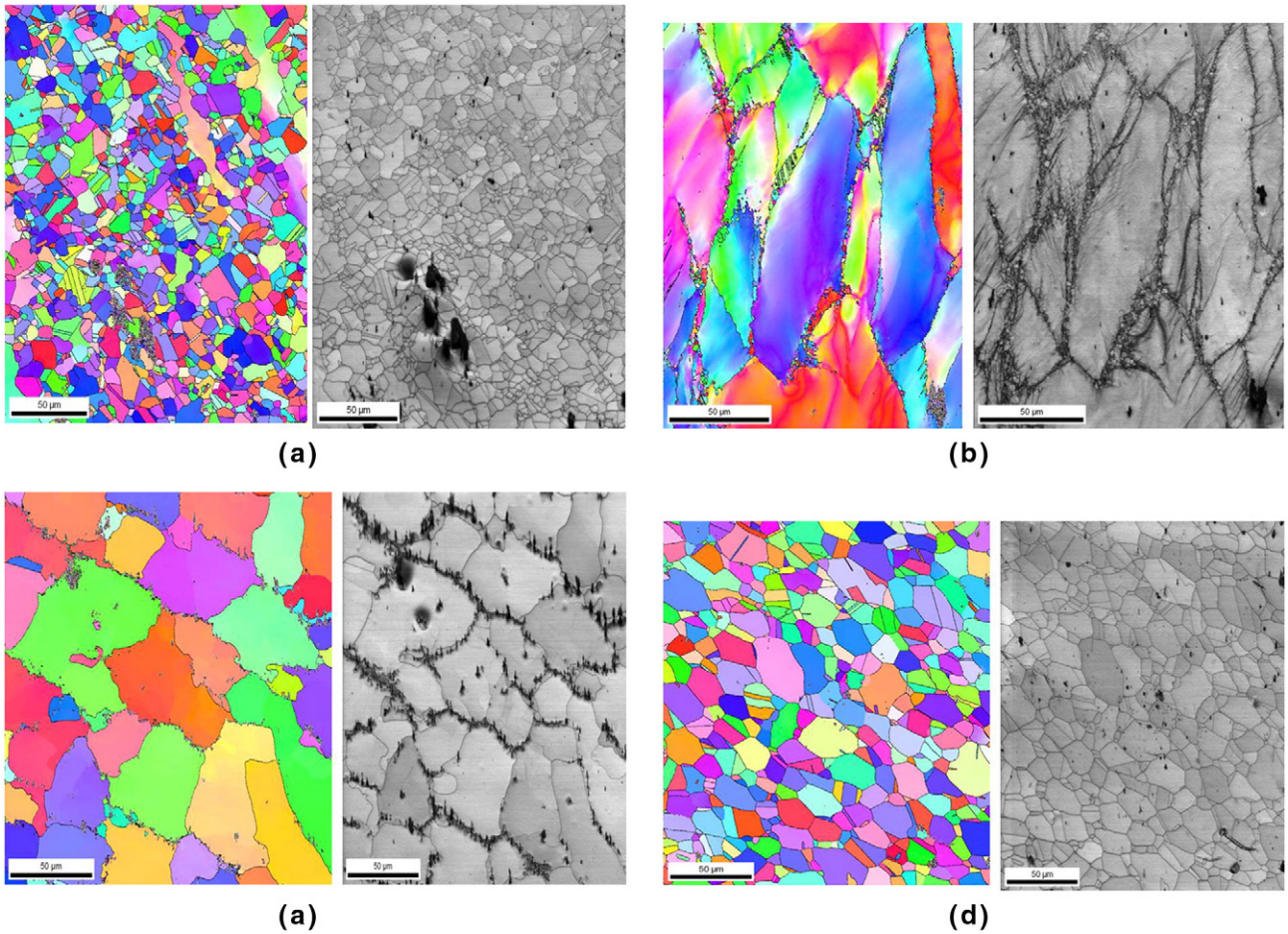

Fig. 7. Inverse Pole Figure and Image Quality map of In718 sample deformed at (a) 950 °C at 10^{-2} s^{-1} (b) 950 °C at 1 s^{-1} (c) 1100 °C at 10^{-2} $s^{-1}$and (d) 1100 °C at 1 s^{-1}.

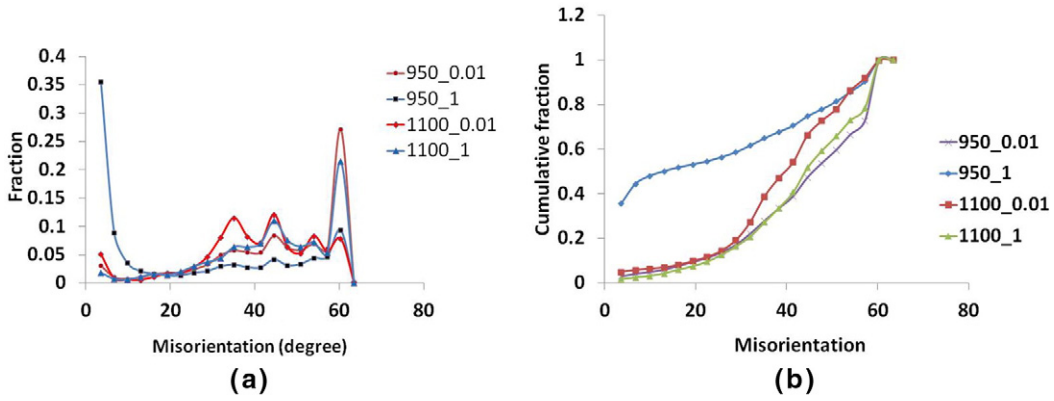

Fig. 8. (a) Misorientation distribution and (b) cumulative misorientation distribution for the deformed IN718 samples. The identification given in the inset corresponds to temperature (°C) and strain rate (s^{-1}) respectively.

interior of the grains and localized shear bands are also observed. The microstructural features depict non uniform deformation.

On the other hand, the microstructures (Fig. 5 (b) and (d)) of specimens deformed at 950 °C and 1000 °C at strain rates of 0.01 s^{-1} are characterized by grains much smaller than the undeformed sample. The microstructure can be characterized by wavy grain boundaries. This is indicative of dynamic recrystallisation of the material where a completely new microstructure evolves out having grains surrounded by clear grain boundaries. It can be observed that dynamic recrystallization has occurred uniformly throughout the grains. The microstructure of samples deformed at 1050 °C and 1100 °C are shown in Fig. 6(a–d). It is clearly evident that the uniform recrystallization throughout the sample has taken place. Hence, dynamic recrystallization is the structural softening mechanism responsible for the decreasing flow stress at higher temperatures. It can be clearly observed that samples deformed at high strain rates (1 s^{-1}) have finer grains (Fig. 6(a) and (c) compared to low strain rates (0.01 s^{-1}) Fig. 6(b) and (d). The finer structure may be due to pinning of grain boundaries by δ phase whereas at lower strain rates it starts dissolving and grain coarsening takes place. Grain coarsening during DRX is found above 1150 °C (Fig. 6). Furthermore, at temperatures above 1050 °C, grain growth occurs at lower strain rates.

3.3. EBSD analysis

Fig. 7 shows the inverse pole figures and image quality maps (IPF and IQ) for the plane strain compression tested IN718 samples. It can be observed that the microstructure shows dynamically recrystallized grains with the exception of sample deformed at 950 °C 1 s^{-1}. The IPF maps show very little change in colour within the grains indicating lower intragranular misorientation and a completely recrystallized microstructure. This observation is corroborated by the misorientation and cumulative misorientation plot of the deformed samples (Fig. 8 a and b). With the exception of the sample deformed at low temperature and high strain rate, all the samples show higher fraction of HAGB. The microstructure is characterized by the presence of twins for the sample deformed at lower temperature and low strain rate and the sample deformed at higher strain rate and higher temperature. It can be concluded that at higher temperature and lower strain rate, twins grow and this contributes to gradual deviation from the twin boundary character to a high angle boundary thereby decreasing the fraction of twin boundaries. This result is further corroborated by the highest fraction of sigma 9 boundaries in this sample compared to other samples (Fig. 9). It is well known that sigma 3 boundaries can react with each other to form sigma 9 boundary. With the progress of recrystallization, grains with random HAGB may consume the twins and lead to a reduction in sigma 3 boundary content in the sample. At lower temperatures and higher strain rates, recrystallization is retarded and therefore, recrystallization twinning is impeded contributing to lower fraction of twin boundaries.

Intragranular misorientation in terms of KAM (Fig. 10) also indicates similar trend with lower dislocation content in the sample deformed at higher temperature or lower strain rate. The sample deformed at the lowest temperature and highest strain rate shows higher KAM value indicating a well developed dislocation structure. Further, the average misorientation of all samples reveals similar trend. The sample deformed at higher strain rate and lowest temperature shows lowest average value indicating larger fraction of low angle grain boundaries. The

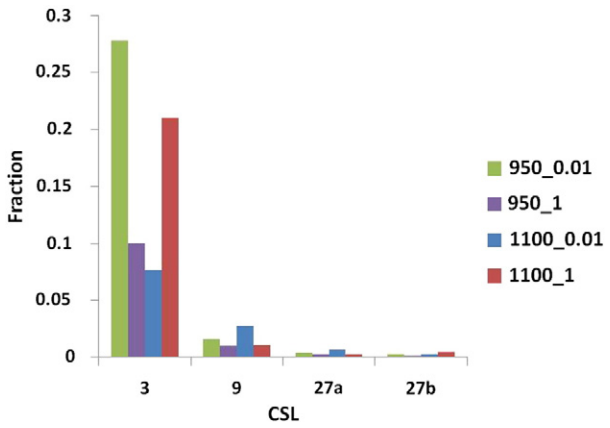

Fig. 9. CSL fraction of IN718 samples. The identification given in the inset corresponds to temperature (°C) and strain rate (s^{-1}) respectively.

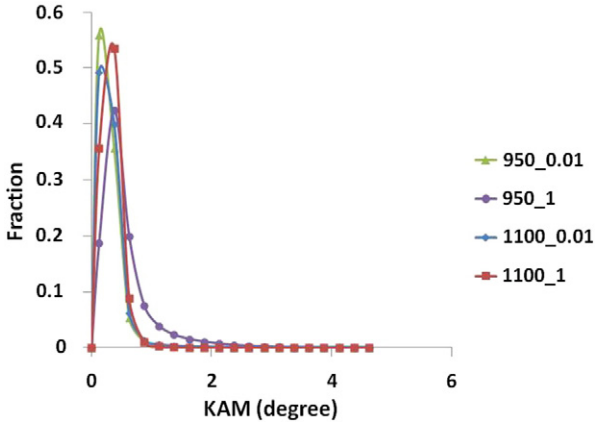

Fig. 10. Kernel Average Misorientation (KAM) distributions. The identification given in the inset corresponds to temperature (°C) and strain rate (s^{-1}) respectively.

Zener–Holloman parameter predicts the deformation behaviour of materials in a lucid way and even gives information about microstructural features like grain size. However, a detailed microstructural analysis indicates that finer details in microstructure like grain boundary character cannot be completely understood with this parameter. The presence of twinning during DRX affects the microstructural evolution and in turn can affect the constitutive behaviour of the material.

4. Conclusions

Isothermal hot PSC tests on Inconel 718 to a true strain of 1.2 indicate dominant role of dynamic recrystallization over a temperature range of 950–1100 °C and at strain rates of 0.01 and 1 s^{-1}. Only the sample deformed at 950 °C and strain rate of 1 s^{-1} shows dynamic recovery. Thus at higher strains dominant in PSC, dynamic recrystallization regime is expanded in the temperature-strain rate space at the expense of dynamic recovery regime. However, the complex state of stress and the role of twinning in dynamic recrystallization needs further investigation. Nevertheless, the present investigation clearly indicates a direct advantage of single step large strain rolling reduction for Inconel alloy IN718.

Acknowledgments

The authors wish to thank Director, VSSC for granting permission to publish this work.

References

[1] D. Benjamin, C.W. Kirkpatrick, Properties and Selection: Stainless Steels, Tool Materials and Special Purpose Metals, ASM International, (OH), 1980.
[2] ASM Metals Handbook, Properties and Selection: Irons, Steels, and High-Performance Alloys, vol. 1, Metals Park, OH, USA, 1990 1.
[3] N. Thadhani, A. Mutz, T. Vreeland Jr., Structure/property evaluation and comparison between shock-wave consolidated and hot-isostatically pressed compacts of RSP pyromet 718 alloy powders, Acta Metall. 37 (1989) 897–908.
[4] K.-M. Chang, M. Henry, M. Benz, Metallurgical control of fatigue crack propagation in superalloys, JOM 42 (1990) 29–35.
[5] L. Geng, Y.-S. Na, N.-K. Park, Precipitation behavior of hot-extruded alloy 718 during isothermal treatment, Met. Mater. 5 (1999) 389–393.
[6] N. Park, I. Kim, Y. Na, J. Yeom, Hot forging of a nickel-base superalloy, J. Mater. Process. Technol. 111 (2001) 98–102.
[7] F.-L. Sui, L.-Q. Chen, X.-H. Liu, L.-X. Xu, Application of FEM to hot continuous rolling process for Inconel 718 alloy round rod, J. Iron. Steel Res. Int. 16 (2009) 43–49.
[8] J. Zhang, Z. Gao, J. Zhuang, Z. Zhong, P. Janschek, Strain-rate hardening behavior of superalloy IN718, J. Mater. Process. Technol. 70 (1997) 252–257.
[9] S. Medeiros, Y.V.R.K. Prasad, W. Frazier, Microstructural modeling of metadynamic recrystallization in hot working of IN 718 superalloy, Mater. Sci. Eng., A 293 (2000) 198–207.
[10] N. Srinivasan, Y.V.R.K. Prasad, Microstructural control in hot working of IN-718 superalloy using processing map, Metall. Mater. Trans. A 25 (1994) 2275–2284.
[11] A. Watts, H. Ford, On the basic yield stress curve for a metal, Proc. Inst. Mech. Eng. 169 (1955) 1141–1156.
[12] C. Sellars, J. Sah, J. Beynon, S. Foster, Plane strain compression testing at elevated temperatures. Report on research work supported by Science Research Council grant B/RG/1481, University of Sheffield, 1976.
[13] S.V.S. Narayana Murty, S. Torizuka, K. Nagai, Microstructural and micro-textural evolution during single pass high Z-large strain deformation of a 0.15 C steel, ISIJ Int. 45 (2005) 1651–1657.
[14] S.V.S. Narayana Murty, S. Torizuka, K. Nagai, N. Koseki, Y. Kogo, Classification of microstructural evolution during large strain high Z deformation of a 0.15 carbon steel, Scr. Mater. 52 (2005) 713–718.
[15] S.V.S. Narayana Murty, S. Torizuka, K. Nagai, Microstructural evolution during simple heavy warm compression of a low carbon steel: development of a processing map, Mater. Sci. Eng. A 410 (2005) 319–323.
[16] E. Puchi, M. Staia, Mechanical behavior of aluminum deformed under hot-working conditions, Metall. Mater. Trans. A 26 (1995) 2895–2910.
[17] E. Puchi, M. Staia, High-temperature deformation of commercial-purity aluminum, Metall. Mater. Trans. A 29 (1998) 2345–2359.
[18] K. Schotten, W. Bleck, W. Dahl, Modelling of flow curves for hot deformation, Steel Res. 69 (1998) 193–197.